Photopolymerization of ceramic/zeolite reinforced photopolymers: towards 3D/4D printing and gas adsorption applications

Yijun Zhang, Yuanyuan Gao, Laure Michelin, Ludovic Josien, Loïc Vidal, Gautier Schrodj, Angélique Simon-Masseron, Jacques Lalévee

Photopolymerization of ceramic/zeolite reinforced photopolymers: towards 3D/4D printing and gas adsorption applications

Yijun Zhang[a,b], Yuanyuan Gao[a,b], Laure Michelin[a,b], Ludovic Josien[a,b], Loïc Vidal[a,b], Gautier Schrodj[a,b], Angélique Simon-Masseron[a,b*], Jacques Lalevée[a,b*]

[a]Université de Haute-Alsace, CNRS, IS2M UMR 7361, F-68100 Mulhouse, France

[b]Université de Strasbourg, France

***Corresponding author:**

Angélique Simon-Masseron, angelique.simon-masseron@uha.fr

Jacques Lalévee, jacques.lalevee@uha.fr,

ABSTRACT

Normally, 3D printed objects *via* photopolymerization usually don't have fully optimized mechanical properties and functions. In this context, the addition of single filler usually can improve these properties through the access to composite materials. However, the addition of filler inevitably has a negative influence on the light penetration inside the composites strongly reducing the depth of cure. Hence, the fabrications of photo-composites based on a combination of two inorganic fillers (alumina Al_2O_3 and zeolite LTA-5A) are reported in this work. Compared to pure poly(ethylene glycol) diacrylate (PEGDA) and its other corresponding single filler-based composites, PEGDA with 25 wt% LTA-5A and 25 wt% Al_2O_3-200 had several improved properties: better depth of cure (DOC), good mechanical properties (the storage modulus, tensile strength, the Young's modulus). Direct laser write (DLW) was used to manufacture 3D patterns and 3D cross-shaped objects with good resolution. Under the hydrothermal stimuli, a 4D printing behavior (reversible shape change) was observed on the 3D cross-shaped objects. In addition, the 3D object with the condition of 4D printing had the ability of withstand a heavy stuff (the mass difference was more than 100 times). This is the first time to report the fabrication of the double

filler-based (50 wt%) composite (ceramic and zeolite) with 4D printing behavior and good mechanical properties. Interestingly, calcinated composites had a certain structure strength and good CO_2 adsorption performance. Therefore, this work not only paves the way for the investigation of photo-composites filled with multiple fillers combinations (how to improve the mechanical properties and keep good depth of cure for composites *via* photopolymerization), but also shows us the potential applications in the field of 3D/4D printing, microlithography and functional composites.

Keywords: Zeolite, Al_2O_3, Photopolymerization, 3D/4D Printing, CO_2 adsorption

1. Introduction

3D printing, also known as additive manufacturing (AM), has been a very inseparable role in human daily life and industrial production [1]. This technology was developed in the 1980s through the concept of stereolithography (SLA) [2]. With the advantage of 3D objects manufacturing with complex spatial resolution, 3D printing has developed rapidly in the last few years, and has been applied in numerous fields, such as biomedical engineering, automotive and aerospace industries, and industrial design, etc. [1, 3-8]. As an important application of 3D printing, 4D printing is with the addition of time as the fourth dimension [9-11]. The structure or function of the 3D object can be changed with time under stimuli from temperature, water, light, electricity [12, 13]. Based on the development of 3D printing, 4D printing can be used for smart textiles, smart devices and biomedical application [14-17].

Photopolymerization has its unique advantages or merits, such as absence of organic solvents as volatile organic compounds (VOCs), low energy consumption, safe optical source, and good temporal and spatial control, which are difficult to be achieved by thermal polymerization [1, 18-21]. Therefore, polymers obtained *via* photopolymerization have been more and more popular in the 3D printing field [22-25]. However, the lack of excellent mechanical properties and functions of pure polymers has limited its developments [2]. The development of different types of fillers has attracted researchers' attention, and many works in developing printable composite materials *via* photopolymerization and reinforced by particles, fibers, and nanomaterials have been reported [1, 2, 26, 27]. Normally, photopolymerizable filled suspensions are composed of fillers, monomers

and photoinitiators [1, 2]. Under light irradiation, photoinitiators generate free radicals into suspension and results in free radical photopolymerization of the monomers in the formulation. Therefore, the polymer matrix is formed and fillers inside are trapped to form composites [28].

Zeolites are microporous crystalline aluminosilicates with a high specific surface area [29]. These molecular sieves have a lot applications in the fields of adsorption [30, 31] and separation, catalytic [32], and medical engineering [33]. Simultaneously, more and more researches reported about polymeric composites containing zeolites, which could improve the functions of composites [31, 34-36]. Zhang et al. [30] used LTA-5A zeolite raw powder, bentonite and photosensitive resin to obtain hierarchical zeolite monoliths by digital light processing (DLP) technique, which can be used for CO_2 adsorption. Halevi et al. [37] manufactured 3D object composites with porous structures containing 50 wt% zeolite 4A via DLP. These 3D monoliths had a high affinity for Cs^+ and Sr^{2+}. Simultaneously, these monoliths retained their porosity, shape and mechanical integrity in aqueous media. Hence, these monoliths can be used to remove radionuclides from nuclear wastewater and for other aqueous separation-based applications. Okulus et al. [38] used the modified zeolite powders as active fillers to prepared dental composites via photopolymerization. Composites containing calcium form of zeolites proved the good ability to release calcium ions during incubation in saline in the amount comparable to calcium phosphates-filled composites, or even higher than dental glass-filled composites. Therefore, these composites can have dental potential applications. In our previous work [26], we prepared zeolite filled composites (~95 wt%) successfully. These formulations can be used for 3D printing through direct laser write or layer-by-layer molding. These composites had improved mechanical properties (the storage modulus) and their corresponding calcinated samples kept the porosity and can be used for CO_2 adsorption and water adsorption.

Ceramic powder is a type of common particles, with the characteristics of high hardness, high melting point and wear resistance. The common ceramics are aluminium oxide (Al_2O_3) [39, 40], zirconium dioxide (ZrO_2) [41, 42], and titanium dioxide (TiO_2) [43], etc. In the recent years, ceramic-polymer composites were widely investigated for their enhanced thermal, mechanical, and functional properties [44, 45]. Xing et al. [39] successfully prepared a UV-curable suspension containing Al_2O_3 (75 wt%), with the presence of diluent and surfactant. Although the solid content was 75 wt%, the depth of cure (DOC) for the composite was less than 0.22 mm, which means this

formulation cannot have a good photopolymerization in depth. Wieclaw- Midor et al. [46] used the heterogeneous nucleation and growth processing to obtain core shell particles based on alpha Al_2O_3 core with silica layer, and these particles were used as filler (20 vol%) in photosensitive resin. After photopolymerization, the presence of silica layer improved DOC of photopolymerizable ceramic dispersion around 20%. Yun et al. [40] coated a silane coupling agent (VTES, vinyltriethoxysilane) onto the surface of Al_2O_3, and then this type of particle was used as filler (0 - 20 wt%) to reinforce the photopolymer. The results shown than tensile characteristics (tensile strength and Young's modulus) were enhanced when the Al_2O_3 ceramic content was 15 wt%. Song et al. [41] prepared high-viscosity ZrO_2 (50 vol%) nanocomposite resins for supportless stereolithography (SLA). However, DOCs of these composites were all less than 240 μm.

In general, the presence of ceramic filler can improve the mechanical properties of polymer, and compared to ceramic based composite, the presence of zeolite can give composite a better depth of cure. Hence, in this work, ceramic/zeolite (Al_2O_3-90 powder, Al_2O_3-200 powder, ZrO_2 powder, LTA-5A and FAU-13X) and monomers (Poly(ethylene glycol) diacrylate (PEGDA), 1,6-Hexanediol diacrylate (HDDA), trimethylolpropane triacrylate (TMPTA)) were used to prepare different types of composites (single filler-based composites and double filler-based composites) through photopolymerization (405 nm, mild conditions under air). The polymerization results were evaluated through the depth of cure (DOC), scanning electron microscopy (SEM), dynamic thermomechanical analysis (DMA), tensile tests, thermogravimetric analysis (TGA). Furthermore, the direct laser write (DLW) was applied to manufactured 3D patterns and cross-shaped objects, which had good spatial resolution. During water swelling property tests, the 3D cross-shaped objects had a good 4D printing behavior. N_2 and CO_2 sorption tests were performed to evaluate textural and adsorption capacity of calcinated composites.

2. Experimental section

2.1 Materials

The oligomer Poly(ethylene glycol) diacrylate (PEGDA, Mw ≈ 600) was purchased from Sartomer (SR610). The monomer 1,6-Hexanediol diacrylate (HDDA), trimethylolpropane triacrylate (TMPTA), the photoinitiator 2-benzyl-2-(dimethylamino)-4'-morpholinobutyrophenone

(BDMK) and solvent acetone were purchased from Allnex or Sigma-Aldrich and used as received and their corresponding molecular structures are shown in Scheme S1. The LTA-5A zeolite powder (code in this work: LTA) and FAU-13X powder (code in this work: FAU) used as fillers were bought respectively from ACROS ORGANICS and Sigma-Aldrich, and used as received. Their characteristics and morphologies are reported in Fig. S1 and Table S1. The ceramic powder Al_2O_3-90 (code in this work: A90), Al_2O_3-200 (code in this work: A200), ZrO_2 powder (code in this work: Z) were bought from CONDEA or PROLABP respectively and used as received. The morphologies of ceramic powders are reported in Fig. S1. The difference between Al_2O_3-90 and Al_2O_3-200 is the surface area values, which are 90 and 200 $m^2 \cdot g^{-1}$ respectively. Depending on the high water adsorption capacity, LTA-5A powder was dried at 120 ^oC overnight, then was used as filler for photopolymerization, and the code of LTA-5A after this process was LTA-5A-Dry.

2.2 Composite preparation

Firstly, the monomer/oligomer (99 wt%) and BDMK (1 wt%) were mixed together to prepare homogenous photosensitive liquid resin mixture by SpeedMixer (DAC 152.1 FVZ-K) with a rotation speed at 1500 rpm/min. Then, the resin mixture (50 wt%) and fillers (50 wt%) were added into a vial to obtain homogeneously dispersed filled resins by SpeedMixer with a rotation speed at 2000 rpm/min. Then the resins were stored in the dark to avoid exposure to light. The basic formulation of composites is presented in Table S2.

The cured composites were prepared in a LED-curing box upon the irradiation of the visible UV light (405 nm, 1 W/cm^2) for 30 s (see Scheme 1.a). Then, the cured composites were cleaned by acetone to remove the unpolymerized part and the depth of cure (DOC) for the cured composite was measured by an Absolute LCD Digimatic Indicator (Mitutoyo). The specific format of a composite code is Monomer-filler content-filler type, e.g., PEGDA-35%LTA-15%A200 means that the composite is generated from the photopolymerization of PEGDA with 35 wt% LTA-5A and 15 wt% Al_2O_3-200.

2.3 Direct Laser Write (DLW)

The homogeneously filled resins were deposited onto a homemade glass tank (2 mm thickness). Then a computer-controlled and programmed laser diode (Thorlabs with 405 nm) with spot size around 50 μm was used for spatial controlled irradiation to produce specific 3D patterns (see Scheme 1.b).

After the process of DLW, these 3D patterns were cleaned by acetone to remove the uncured monomer. Finally, the printed 3D patterns were observed through a numerical optical microscope (NOM) (DSX-HRSU, OLYMPUS Corp). As the color pattern morphology shown in Fig. S2, it can be observed that these 3D patterns remained well resolved and their surface were very flat. Therefore, the results of NOM images clearly indicated that these composites can be prepared with excellent spatial resolution.

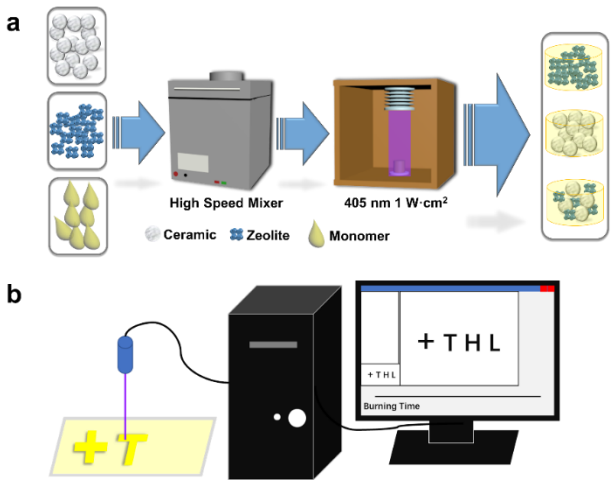

Scheme 1. Process for (a) preparing composite and (b) direct laser write (DLW).

2.4 Calcination

Samples PEGDA-50%LTA-0%A200, PEGDA-25%LTA-25%A200, PEGDA-35%LTA-15%A200, and PEGDA-0%LTA-50%A200 were calcinated at 750 ^{o}C under air (heating rate at 1 ^{o}C/min, without air flow) during 4 h to obtain their corresponding white samples. After calcination, the shape and structure of calcinated samples could remain intact, compared to their corresponding composites before calcination. In this work, the code of calcinated sample is Monomer-filler content-filler type-calcination time. For example, PEGDA-35%LTA-15%A200-4h, means that PEGDA-35%LTA-15%-A200 composite was calcinated at 750 ^{o}C for 4 h, and LTA-5A-4h means that LTA-5A powder after drying treatment was calcinated at 750 ^{o}C for 4 h.

2.5 Material characterization

The ceramic and zeolite particle sizes, their morphology, and their corresponding composites including any macroporosity present in samples were investigated by scanning electron microscope (SEM, FEI Quanta 400 and JEOL JSM-7900F). Thermogravimetric analyses (TGA) were performed using a METTLER-TOLEDO TGA/DSC 3+ thermoanalyzer. 30 mg samples

were heated from 30 to 500 °C at a heating rate of 10 °C/min under nitrogen atmosphere (purge of 100 mL/min of N_2 protection gas).

For dynamic thermomechanical analysis (DMA), composites were polished to obtain a pellet with a thickness of 1 mm, and then experiments were performed on Viscoanalyser METTLER DMA861 at a frequency of 1.00 HZ. For tensile tests, composites were prepared into dumbbell-like samples (1 mm thickness) and were tested by modernized Dynamometer INSTRON 4505 to evaluate the tensile strength and tensile strain.

After direct laser write (DLW), 3D cross-shaped objects were obtained and then water swelling property characterization was performed on these objects. These samples were submerged in distilled water at room temperature (25 ^{o}C, 8 h). Then, these samples were taken out periodically and water was wiped out on their surfaces. Samples were weighted immediately by a precise four-digit balance to measure the content of absorbed water. The percentage of water was calculated by the equation (1):

$$R = {(m_2 - m_1)}/{m_1} \times 100\% \quad (1)$$

Where m_2 is the weight of the sample after water swelling, and m_1 is the weight of the dried sample.

At room temperature, ^{27}Al MAS NMR analysis was performed on a Bruker AVANCE NEO 400WB spectrometer at B_0 = 9.4T (Larmor frequency ν_0 = 104.23 MHz), a proton $\pi/12$ pulse length of 0.36 μs and a recycle delay of 1s. All the measurements were carried out with $[Al(H_2O)_6]^{3+}$ as an external standard reference. ^{29}Si Single pulse magic angle spinning (SPE-MAS) experiments were performed with a Bruker Avance II 300 MHz spectrometer operating at B_0 = 7.2 T (Larmor frequency ν_0 = 59.62 MHz) equipped. During the analysis process, a spinning rate of 4 kHz, a pulse angle of $\pi/6$ (2.03 μs) and a recycling delay of 80 s were used at room temperature. The relative proportions of the different Q^n Si species were ensured by the recording conditions.

The crystalline structures of fillers were identified by X-ray diffraction (XRD) measurements using a PANalytical MPD X'Pert Pro diffractometer operating with Cu Kα radiation (Kα = 0.15418 nm) equipped with an PIXcel real-time multiple strip detector (active length = 3.347° (2θ)). The powder patterns were collected at 295 K in the range $3 < 2\theta < 70$, step = 0.013° (2θ), time/step = 220 s. They were analyzed by using the X'Pert HighScore software package and

compared with documented diffraction patterns in the International Centre for Diffraction Data (ICDD) database.

Nitrogen (N_2) adsorption-desorption isotherms were performed at -196 °C with a Micromeritics ASAP 2420 Instrument on calcinated samples and pure filler powder in order to determine their micro- and mesoporous characteristics. Before each measurement, the samples were outgassed to a residual pressure of less than 0.8 Pa at 90 °C for 1 h and 300 °C for 15 h. Specific surface areas were calculated according to the Brunauer-Emmett-Teller (BET) method ($0.01 < p/p^0 < 0.03$). The *t*-plot method was used to calculate microporous volume (V_{micro}) and microporous surface area (S_{micro}). The external surface (S_{ext}) was obtained by subtracting S_{micro} from the total surface. Mesopore size distributions were calculated by the Barrett-Joyner-Halenda (BJH) method on the desorption branch of the isotherm.

The CO_2 adsorption capacities of the calcinated samples were achieved at 0 °C with a Micromeritics ASAP 2420 Instrument under 105 Pa. Before each measurement, the samples were outgassed to a residual pressure of less than 0.8 Pa at 90 °C for 1 h and 300 °C for 15 h.

3. Results and discussion

3.1. Characterization of the composites

3.1.1 DOC and DMA for single filler-based composites

The depth of cure (DOC) is a very important property of composites generated by photopolymerization, which is defined as the thickness of materials cured. Normally, the optical properties of composites *via* photopolymerization determine not only their aesthetic appearance, but also their polymerization kinetics and their depth of cure. Due to different textures, geometries and refractive indices of fillers, the light absorption and light scattering have negative influences on the light transmittance inside filled formulations. When light penetrates the interior of mixed formulation, part of light can be absorbed by fillers, which means the light cannot penetrate into the depth of the mixed formulation. For the light scattering, it was affected by the respective refractive indexes of filler and monomer during photopolymerization process but also by the size and shape of the fillers. Normally, compared to polymer, the refractive index of the composite increases due to the increase in the density and reduced polarizability during the period of

photopolymerization, while the refractive index of the fillers remains constant [47]. If the initial refractive index of the monomer is higher than that of the filler, further photo-curing increases the refractive index mismatch, thus progressively decreasing the transmittance. Hence, the change in the transmittance of the composite is a complex phenomenon. In general, the transmittance of composites always decreases with the increasing content of filler [48]. Hence, three different types of monomers and five different types of fillers (two types of zeolites and three types of ceramics) were evaluated for photopolymerization of composites.

In Fig. 1, the differences in DOCs were observed, according the type of monomer and the type of filler. Firstly, it is obvious to see that composites with zeolites had higher DOC values than that with ceramic fillers, especially LTA-5A zeolite. For ceramic fillers, Al_2O_3-200 had better DOCs than other two ceramic fillers in all types of monomers. This might be due to the different sizes and different particles shape of these fillers, which could have influences on the light scattering and hence the light penetration [49, 50]. In our previous work, LTA-5A and FAU-13X both had good DOCs with high filler content (70 wt% for LTA-5A and 60 wt% FAU-13X), and some 3D patterns with flat surface can be obtained via DLW.[34] In this work, as shown in Fig. S1, LTA-5A (2.0 μm) and FAU-13X (2.7 μm) both have smaller particle sizes than two types of Al_2O_3 particles (both around 10-20 μm), and ZrO_2 has aggregations (around 20 μm) of particles with undefined shape (around 2-4 μm) (see Fig. S1). Hence, smaller particle sizes of filler and no particle agglomeration can improve the light penetration and help composite to have a better DOC, e.g., LTA-5A and FAU-13X.

Secondly, when three different types of monomers or oligomer (PEGDA, TMPTA and HDDA) were evaluated, PEGDA matrix composites had higher DOCs than other monomer-matrix composites at the same filler content. It is because zeolites and ceramics are all hydrophilic as PEGDA. Thus low-molecular weight PEGDA can play the role of hydrophilic dispersant. This means that the fillers and PEGDA monomer based formulations are all hydrophilic. This mixture is more stable and obtained with efficient mixing condition which helps PEGDA based formulations to be more homogenous for light penetration during photopolymerization.

Normally, well dispersed inorganic filler with good interactions with polymeric matrix improve the storage modulus (G'), because of the stiffness of inorganic filler and the increase of constrains of the segmental motions of the polymeric chain in the network [34, 51]. Therefore,

dynamic thermomechanical analysis (DMA) was carried on PEGDA matrix composites with different types of fillers, due to PEGDA matrix composites have a higher DOC value than that of other composite. As shown in Fig. 1.d, the storage modulus (G') values of composites with different types of fillers are all larger than that of the pure PEGDA (5.7 MPa), and PEGDA-50%A200 has the highest G' value (52.0 MPa), increasing by 812%. This can be explained by the excellent stiffness of Al_2O_3, which can significantly reinforce the storage modulus. PEGDA-50%A90 has the second highest G' values (32.0 MPa), increasing by 450%, which is related to the different surface area values. Because higher surface area can increase both interfacial and filler-filler interactions leading to substantial mechanical property improvement [52]. Simultaneously, compared to pure PEGDA, the G' value of PEGDA-50%LTA increases by 250%. Therefore, these fillers can improve the mechanical properties of PEGDA and Al_2O_3-200 particles lead to better mechanical properties than zeolites.

Single filler-based composites have their unique performances: LTA-5A based composites have the higher value of the depth of cure (DOC), and composites containing Al_2O_3-200 have better mechanical properties. Hence, double filler-based composites (zeolite/ceramic: LTA-5A and Al_2O_3-200) were studied in the following steps.

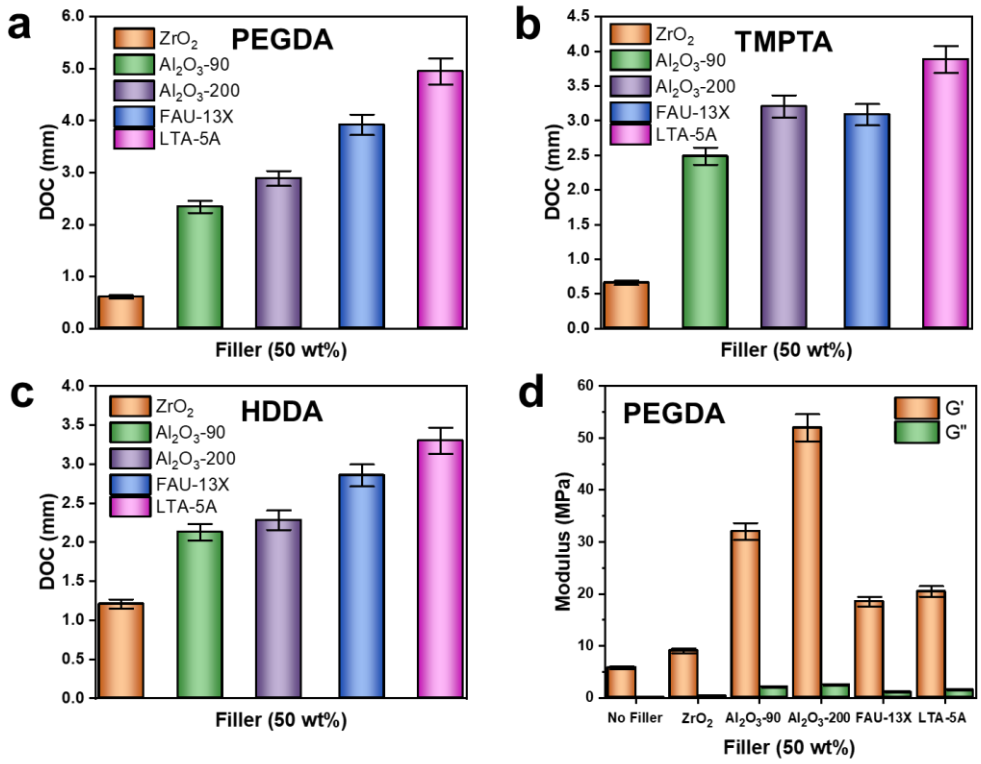

Fig. 1. DOC and DMA for different single filler-based composites (LED@405nm, 1 W/cm^2 for 30 s): (a) PEGDA containing 5 different types of filler; (b) TMPTA containing 5 different types of filler; (c) HDDA containing 5 different types of filler. (d) DMA for PEGDA containing 5 different types of filler.

3.1.2 DOC and DMA for zeolite/ceramic-based composites

In order to estimate DOCs for zeolite/ceramic blends, Al_2O_3-200 and LTA-5A were blended at different ratios (see Table S2). The total content of filler was kept at 50 wt% (vs. organic resin). As shown in Fig. 2.a, DOCs of these composites decrease from 4.9 mm to 2.9 mm with the decrease of the LTA-5A content from 50 wt% to 0 wt%. Hence, the presence of LTA-5A in Al_2O_3-200 filled composites improved obviously the DOCs.

Compared to PEGDA-50%LTA (G'= 20.4 MPa), when Al_2O_3-200 was blended with LTA-5A in PEGDA, the G' values of these composites strongly increase with the increase of the Al_2O_3-200 content (see Fig. 2.b). Compared to PEGDA-50%LTA and pure PEGDA, the storage modulus (G') values of PEGDA-25%LTA-25%A200 is increased by 20 % and 345 % respectively.

Depending on these results, when the blend of Al_2O_3-200 and LTA-5A is used as filler, the corresponding composites have improved mechanical properties and good DOCs compared to pure PEGDA polymer.

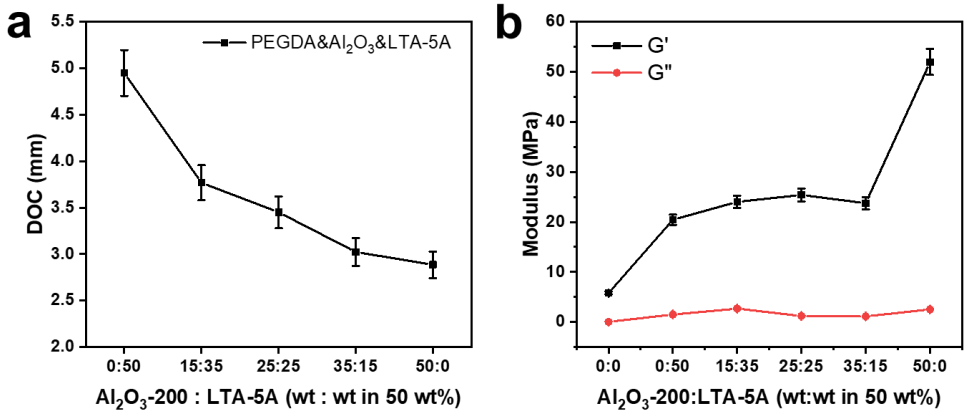

Fig. 2. (a) DOC and (b) DMA for two fillers-based composites with different [Al_2O_3-200] : [LTA-5A] ratios.

3.1.3 Tensile tests

The composites with a blend of Al_2O_3-200 and LTA-5A were characterized by tensile tests experiments. As shown in Fig. 3, the pure PEGDA shows its best value of tensile strain (9.3 %), the lowest value of tensile strength (1.8 MPa) and the lowest value of Young's modulus (23.1

MPa). Composite with only Al_2O_3 have the best mechanical properties (the highest Young modulus). When Al_2O_3-200 was blended with LTA-5A, the tensile strain values of these composites increase from 2.4 % to 6.2 %, and the values of tensile strength decrease from 4.5 MPa to 3.4 MPa, with the increased LTA-5A content from 0 wt% to 50 wt% (Fig. 3.b). The tensile strength values of PEGDA-25%LTA-25%A200, PEGDA-15%LTA-35%A200 and PEGDA-50%A200 are all around 4.5 MPa, while the DOC value of PEGDA-25%LTA-25%A200 is higher than that of PEGDA-15%LTA-35%A200 and PEGDA-50%A200 respectively. The decreased ductility (tensile strain) of these samples results from the increasing Al_2O_3-200 content, which helps to increase the rigidity and withstand higher stresses.[51] In addition, the values of Young's modulus also have a decreasing tendency from 233.9 MPa to 87.1 MPa, with the increasing content of LTA-5A from 0 wt% to 50 wt% (Fig. 3.c), Then, compared to pure PEGDA polymer, the presence of ceramic and zeolite fillers enhance the tensile strength and Young's modulus obviously i.e. ceramic fillers lead to higher Young's modulus than zeolite in agreement with the trend found above for G' in DMA measurements.

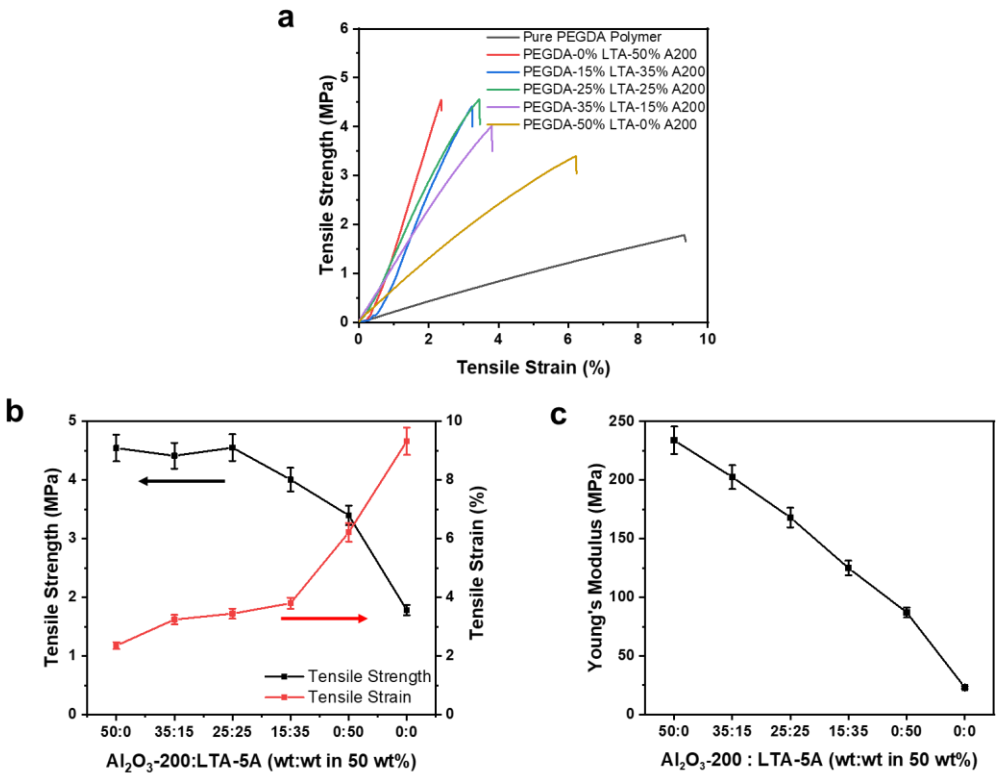

Fig. 3. Tensile tests for PEGDA matrix composites with different [Al_2O_3-200] and [LTA-5A] ratios: (a) and (b) of tensile strength and tensile strain, and (c) Young's modulus.

3.1.4 Interfacial morphology

The interfacial morphologies of composites were analyzed by scanning electron microscope (SEM). The main morphological characteristics of different types of fillers are shown in Fig. S1. LTA-5A (Fig. S1.a) and FAU-13X (Fig. S1.b) are characterized by well-shaped cubic morphology (2 μm) and twinned octahedra reveal (2.7 μm) respectively. About Al_2O_3-90 (Fig. S1.c) and Al_2O_3-200 (Fig. S1.d), they are both spherical particles (around 10-20 μm). For ZrO_2 (Fig. S1.e), an obvious aggregation (around 20 μm) can be observed and the size is around 2-4 μm, and normally the aggregation of particles can lead to degradation in composite strength [53]. SEM images of composites (PEGDA-50%LTA, PEGDA-15%LTA-15%A200 and PEGDA-50%A200) are presented in Fig. S3, including images of surface and cross-section. It is obvious to observe an intimate contact between the fillers and PEGDA matrix in general with a good dispersion. Even when two different types of fillers (LTA-5A and Al_2O_3-200) were added in PEGDA, as well as the homogenous dispersion of fillers can be observed. Hence, the homogeneous dispersion of fillers in PEGDA improved the mechanical properties.

3.1.5. Thermal properties

In order to quantitatively illustrate whether the presence of fillers enhanced the thermal stability of composites, thermogravimetric analyses (TGA) were carried out on composites. As shown in Fig. S4, there are two steps occurring between 50 and 600 ^{o}C, which are 50-300 ^{o}C and 300-600 ^{o}C. The first step (50-300 ^{o}C) is about water desorption, and the values of weight loss (ML-1) of Al_2O_3-200, LTA-5A and PEGDA are 7.3 wt%, 16.7 wt% and 0.1 wt% respectively. The second step (300-600 ^{o}C) corresponds to the carbonization or decomposition of polymer (ML-2). As listed in Table S3, the temperature of the maximum decomposition rate (T_{max}) is slightly reduced by around 15°C by the presence of fillers. Hence, the addition of filler has an effect on the thermal stability of composites. In addition, a good correlation can be observed between ML-2 and the amount of monomer used in the formulation (MN) (see Table S3).

3.1.6 Water swelling property

In order to measure the water swelling properties of composites with double types of fillers, 3D cross-shaped samples were obtained *via* direct laser write (DLW). As shown in Fig. 4.a, the

volume expansion can be observed on these 3D cross-shaped samples after water swelling process for 8 hours. After evaporation at 80 ^{o}C for 1 hour, the pure PEGDA sample was broken and many cracks appeared on its surface. Compared to the pure PEGDA sample, these two composites kept intact as their original shapes and without any cracks on the surfaces in agreement with better mechanical properties for composites vs. pure PEGDA polymer. As observed in Fig. 4.b, the swelling ratio of pure PEGDA sample is 64 wt%, while those of PEGDA-35%LTA-15%A200 and PEGDA-25%LTA-25%A200 are only 33 wt% and 37 wt% respectively, which is approximately half of that of pure PEGDA. This is due to the presence of 50 wt% fillers in composites. Therefore, compared to pure PEGDA, composites also keep the property of water swelling, although the swelling ratio values are lower than for pure PEGDA.

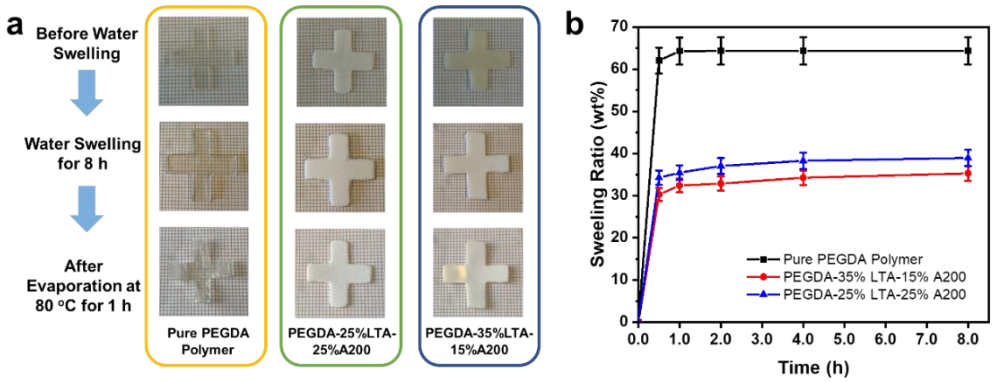

Fig. 4. Water swelling tests of (a) 3D cross-shaped samples. Swelling ratio of 3D cross-shaped samples are summarized in (b).

3.2 4D printing behavior

Based on the 3D printing technology, 4D printing technology has developed rapidly all over the world, which is with addition of time as the fourth dimension [1, 14]. Normally, 4D printing is regarded as giving a printed structure the ability to change its form or function with time (t) under stimuli such as temperature, solvent (e.g. water), light, electricity, and magnetic field [10, 54, 55]. Hence, a 3D cross-shaped object with spatially resolved properties was designed and 4D printing process was performed through the water swelling and dehydration processes of the 3D cross-shaped object (Fig. 5.a).

As shown in Fig. 5.b the cross-shaped object of pure PEGDA obtained after water swelling has an obvious reversible shape change during the evaporation process (80 ^{o}C within 10 min) : the central part of the object was raised (see Video S1 at 4 times speed for 4D printing behavior).

However, there were several cracks appeared on the surface of the pure PEGDA, which were highlighted in red circles. When the same processes were carried on PEGDA-25%LTA-25%A200, the same shaped change was observed and this object was not broken after evaporation process (80 ^{o}C within 10 min) (Fig. 5.c, see Video S2 at 4 times speed). In addition, the same processes could be repeated on PEGDA-25%LTA-25%A200 (Fig. 5.d, see Video S2 and S3 both at 4 times speed for 4D printing behavior). Therefore, the significant 4D printing behavior can be exhibited under the hydrothermal stimuli, and this behavior can be realized for several times (or cycles). This 4D printing is based on hydrophilic property of PEGDA and the light attenuation in depth. The PEGDA based polymers have very good hydrophilic behavior. When PEGDA polymer is introduced into water, a large number of water molecules come to contact with the ethyleneglycol units, causing the polymer to rapidly absorb water. The light attenuation is a common phenomenon in photopolymerization, where the intensity of light decreases with increasing depth resulting in the difference in the cross-linking density in the thickness direction. The rapid water absorption and the difference of cross-linking density result in the change in the volume of the object and a change in the stress inside the object. Hence, 4D printing behavior can be observed.

Due to the good mechanical properties of PEGDA-25%LTA-25%A200, the load-bearing property of the composite with 4D printing status was observed by applying heavy object on it. When a 4D printing behavior appeared completely, a small empty container (2.5 g) was placed on the four-corners of the object (0.13 g), and drops of water was added continuously into the container. These processes are presented in Fig. 5.e. As the total mass of the container increased, the cross-shaped object was gradually compressed and its four-corners gradually fell down. Finally, this object can withstand the mass of 15 g, and when the heavy container was removed, this object kept its 4D printing shape without any damage. The whole process can be observed in Video S4 at 4 times speed. Therefore, this object with 4D printing condition can withstand a heavy stuff (more than 100 times its own mass).

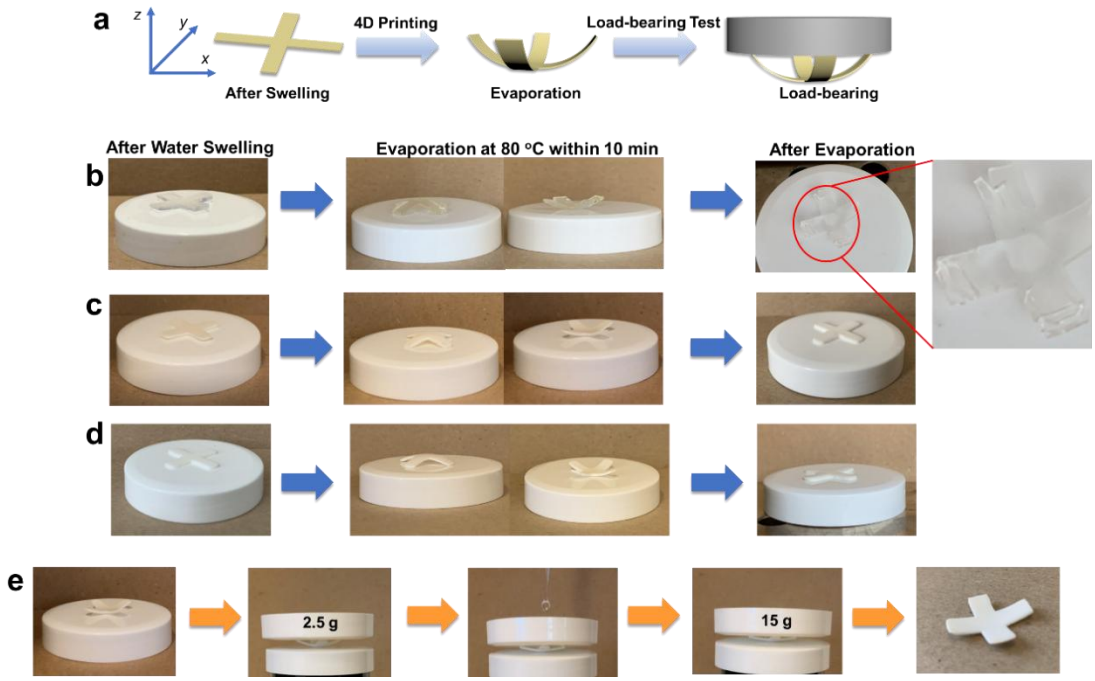

Fig. 5. 4D printing behavior based hydrothermal stimuli. (a) Designed geometrical properties of cross-shaped object and scheme of 4D printing; 4D printing behavior of (b) pure PEGDA polymer, (c) PEGDA-25%LTA-25%A200 (1st cycle), (d) PEGDA-25%LTA-25%A200 (after 2nd cycle), (e) the load-bearing property test of PEGDA-25%LTA-25%A200 with 4D printing behavior.

3.3 Porosity and structure strength of calcinated samples

3.3.1 Solid-state nuclear magnetic resonance (NMR)

In order to check the interaction between LTA-5A zeolite and Al_2O_3-200 ceramic after calcination, solid state NMR was carried out and the results are shown in Fig. 6. The ^{29}Si solid-state MAS NMR spectra of LTA-5A powder, LTA-5A Powder-Dry and LTA-5A-4h, PEGDA-50%LTA-4h and PEGDA-25%LTA-25%A200-4h are shown in Fig. 6.a respectively. For LTA-5A powder, the intense resonance at -91.4 ppm corresponds to the Si atom covalently bonded to four oxygen atoms, referred as $[Si(OAl)_4]Si$ [56]. The second resonance at -96.5 ppm was associated to $[Si(OAl)_2(OSi)_2]Si$ [57]. For LTA-5A Powder-Dry, it has the same Si spectra as LTA-5A powder, which means that drying treatment before photopolymerization did not have significant effect on the crystal structure. However, for LTA-5A Powder-4h, PEGDA-50%LTA-4h and PEGDA-25%LTA-25%A200-4h, the intense resonances of $[Si(OAl)_4]Si$ and $[Si(OAl)_2(OSi)_2]Si$ both have a shift respectively. This could be related to the calcination process which homogenized the silicon environment.

Al atoms were analyzed by ^{27}Al MAS NMR and the results are shown in Fig. 6.b. For LTA-5A powder, the signals at around 50 ppm and 78 ppm correspond to four fold coordinated Al in the framework $Al(OSi)_4$ and extra framework $Al(OH)_4^-$ species. The presence of $Al(OH)_4^-$ can be related to the residual aluminium source during industrial synthesis process [58]. For LTA-5A Powder-Dry, it has the same Al spectra as LTA-5A powder, except for the difference in signal strength, which shows that the drying treatment did not have a significant effect on the framework of LTA-5A. After calcination, the signals of $Al(OSi)_4$ in zeolite framework from LTA-5A Powder-4h, PEGDA-50%LTA-4h and PEGDA-25%LTA-25%Al200-4h all become sharp and shift to 58.5 ppm and 57.5 ppm respectively. It indicates homogenization of Al environment. However, the signal of $Al(OH)_4^-$ disappeared probably because of its transformation into other compounds, such as Al_2O_3 or $NaAl(SiO_4)$ (see section 3.3.2 X-ray diffraction (XRD)) during calcination. For Al_2O_3-200 powder, the position of the NMR lines allows to distinguish the coordination of aluminum atoms : the lines with maxima in the ranges 0-10 ppm and 60-70 ppm should be attributed to four-coordinated AlO_4 and six-coordinated AlO_6, respectively [59]. For PEGDA-25%LTA-25%A200-4h and PEGDA-50%A200-4h, all of these signals have a corresponding overlap with the resonances from Al_2O_3-200 powder.

Based on the results of ^{29}Si and ^{27}Al MAS NMR experiments, the calcination process did not induce a strong interaction between LTA-5A zeolite and Al_2O_3-200. In order to see the consumption $Al(OH)_4$ at 78 ppm, X-ray diffraction (XRD) analyses was performed and presented below.

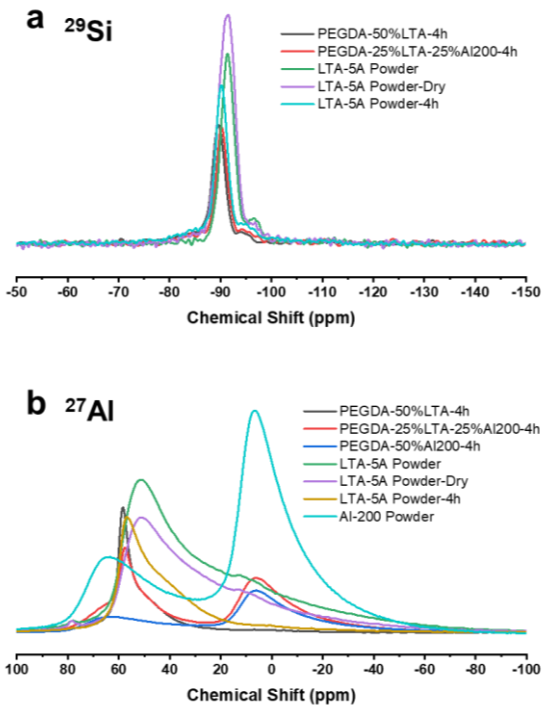

Fig. 6. Solid state nuclear magnetic (NMR) for different samples: (a) ^{29}Si MAS NMR spectra; (b) ^{27}Al MAS NMR spectra.

3.3.2 X-ray diffraction (XRD)

X-ray diffraction (XRD) was performed on LTA powder, LTA powder-4h and PEGDA-50%LTA-4h firstly. As reported in Fig. 7.a, the XRD patterns of these samples are similar respectively to those of the zeolite powder in agreement with the literature (reference card: ICDD 04-009-4857). However, for LTA-5A Powder-4h and PEGDA-50%LTA-4h, the presence of some very weak peaks also can be observed, and these can be related to the FAU zeolite and $NaAl(SiO_4)$ (reference card: ICDD 01-70-4281 and ICDD 04-024-6496, respectively), which could be formed during the calcination process. The formation of FAU zeolite and $NaAl(SiO_4)$ could be related to the consumption of $Al(OH)_4$. Then, XRD also was performed on PEGDA-25%LTA-25%A200-4h and Al_2O_3-200 powder. As shown in Fig. 7.b, Al_2O_3-200 filler in PEGDA-25%LTA-25%A200-4h keep its stable structure during calcination process, which is similar to the reference (reference card: ICDD 01-079-1558). LTA-5A zeolites also keep its crystal structure and the presence of FAU and $NaAl(SiO_4)$ crystals also can observed. Hence, the calcination process does not change the structures of LTA-5A zeolite and Al_2O_3-200 obviously.

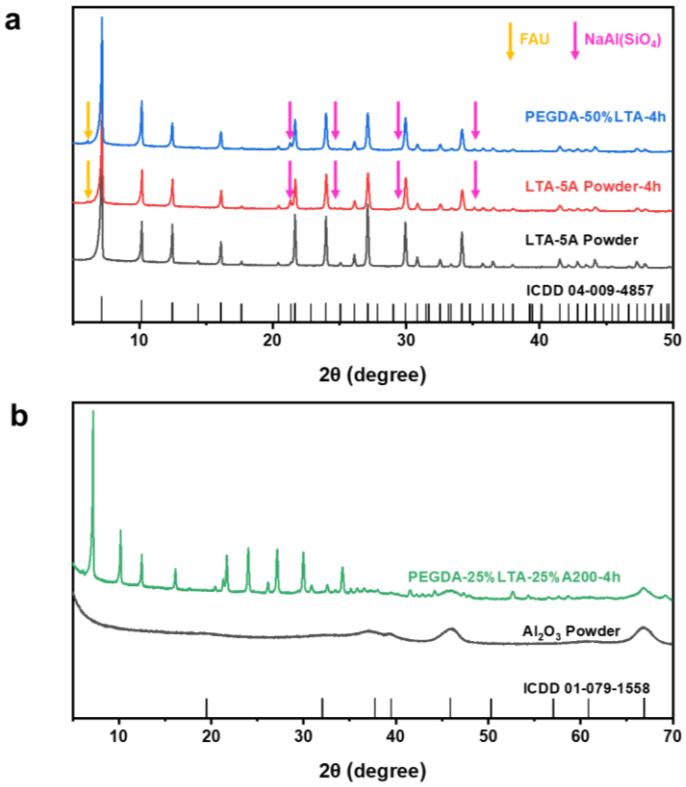

Fig. 7. XRD for (a) LTA-5A powder, LTA-5A powder-4h and PEGDA-50%LTA-4h; (b) Al_2O_3 powder and PEGDA-25%LTA-25%A200-4h.

3.3.3 Porosity estimation and CO_2 adsorption

Nitrogen (N_2) adsorption measurements were undertaken to evaluate the textural properties of calcined samples. The isotherm of LTA-5A powder shown in Fig. 8.a is type I characteristic of microporous compounds. The isotherms of Al_2O_3-200 powder and PEGDA-50%A200-4h are both type IV characteristic of mesoporous compounds with a hysteresis loop (H4 type, relative pressure at 0.6-0.9). Compared to LTA-5A powder, PEGDA-50%LTA-4h has a visible hysteresis loop (H1 type) at relative pressure 0.4-0.8, which reveals the presence of mesopores (diameter at 3.8 nm). This could be related to crystal agglomerates during the calcination process leaded to the formation of mesopores between zeolite crystals. Therefore, double filler-based composites after calcination (PEGDA-35%LTA-15%A200-4h and PEGDA-25%LTA-25%A200-4h) both have the hysteresis loop (H4 type, relative pressure at 0.6-0.9) and mesopores with two diameters at 3.5 nm and 7.6 (7.7) nm. As listed in Table 1, and compared to LTA-5A powder, the microporous surface and volume of PEGDA-50%LTA-4h decrease and the values were reduced by 21.3% and 21.4%, which is related to micropores blocked because of the carbon formed from calcination, and crystal

agglomerates. Compared to Al_2O_3-200, PEGDA-50%A200 has a slightly increased quantity adsorbed, which can be explained that the Al_2O_3 particles agglomerated to form interparticle mesopores (similar to the inside mesopore size of Al_2O_3-200 (7.3-7.5 nm)) during calcination process. For calcined zeolite/ceramic based composites, these two values have an obvious reduce (43.2% and 42.8% for PEGDA-35%LTA-15%A200-4h; 61.4% and 60.7% for PEGDA-25%LTA-25%A200-4h). PEGDA-50%LTA and PEGDA-35%LTA-15%A200 can have higher or similar textural properties compared to LTA-5A commercial beads. Therefore, the interesting porous volumes of calcined samples show the possibility to used them as adsorbents. As shown in Fig. S5, calcination induces particle agglomeration to form also macroporosity (pore diameter $\geq$ 50 nm) with macropores of inhomogeneous size and shape.

The CO_2 adsorption isotherms are shown in Fig. 8.b and these corresponding adsorption capacities ($mmol \cdot g^{-1}$) are listed in Table 1. For these samples, rapid adsorption at low-relative pressure can be observed and it reveals the rapid adsorption in their micropores. The CO_2 uptakes at p/p^0 = 0.03 of LTA-5A powder, PEGDA-50%LTA-4h, PEGDA-35%LTA-15%A200-4h, PEGDA-25%LTA-25%A200-4h and PEGDA-50%A200-4h and commercial LTA-5A beads are 112, 98, 79, 61, 7, 87 $cm^3 \cdot g^{-1}$ respectively. The value for PEGDA-50%LTA-4h is around 12% lower than LTA-TA powder, and this can be explained by the residual carbon blocking partially to micropores. The obviously decreased values of PEGDA-35%LTA-15%A200-4h and PEGDA-25%LTA-25%A200-4h are mainly related to the decrease of the zeolite content, but also to the presence of Al_2O_3 which has a very low CO_2 adsorption capacity. Compared to commercial LTA-5A beads, PEGDA-35%LTA-15%A200-4h and PEGDA-50%LTA show similar or slightly higher CO_2 adsorption capacity. Hence, calcined samples have potential application for CO_2 adsorption.

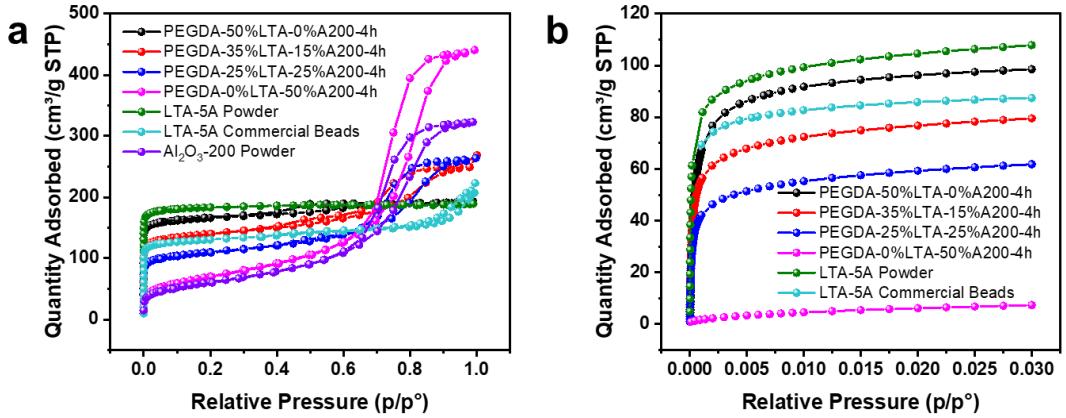

Fig. 8. Isotherms of LTA-5A powder, the corresponding calcined samples and commercial LTA-5A beads: (a) N_2 adsorption-desorption isotherms and (b) CO_2 adsorption isotherm.

Table 1. Textural properties of LTA-5A powder and corresponding calcined composites and commercial LTA-5A beads determined after N_2 adsorption-desorption, and their CO_2 adsorption capacities.

	S_{BET} [$m^2 g^{-1}$]	$S_{external}$ [$m^2 g^{-1}$]	S_{micro} [$m^2 g^{-1}$]	V_{micro} [$cm^3 g^{-1}$]	Mesopore Diameter [nm]	CO_2 Adsorption Capacity (mmol·g^{-1})
LTA-5A Powder (LTA)	746	1	745	0.28	/	4.8
Al_2O_3-200 Powder (A-200)	219	219	/	/	7.5	/
PEGDA-50%LTA-4h	664	78	586	0.22	3.5	4.3
PEGDA-35%LTA-15%A200-4h	554	121	423	0.16	3.5; 7.6	3.5
PEGDA-25%LTA-25%A200-4h	418	131	287	0.11	3.5; 7.7	2.7
PEGDA-50%A200-4h	254	254	/	/	7.3	0.3
LTA-5A Commercial Beads	546	78	436	0.17	20.9; 48.1	3.9

3.3.4 Structure strength of calcinated samples

After calcination, a bear-loading test was carried out on these calcined samples to evaluate their mechanical properties. Standard 50 g or 100 g weights were put on the top surface of calcined samples (sample's weight was kept around 0.1 g) to see whether the structure and shape of these calcined samples change. For PEGDA-50%LTA-4h, when a 50 g weight was put on its top surface, this calcinated block was broken into several parts due to the compression from the weight, which also indicates its good uniformity after calcination (see Fig. 9.a). For PEGDA-35%LTA-15%A200-4h, it could stand the compression from a 100 g weight and kept the structural

integrity (see Fig. 9.b). For PEGDA-25%LTA-25%A200-4h, it could stand a 50 g weights, but a 100 g weights destroyed its structure (see Fig. 9.c). For PEGD-A50%A200-4h, when a 50 g weights was put its top surface, it was destroyed into powder, which meant this sample's fragility and calcination could not give it a good structure strength (see Fig. 9.d). Hence, the use of a small amount of Al_2O_3 can significantly improve the structural strength of the calcinated sample.

As shown in Fig. S5, scanning electron microscope analyses (SEM) were also performed on the calcinated samples to observe their interfacial morphologies. For PEGDA-50%LTA-4h, zeolites have a good distribution and aggregation after calcination process, which allows it to break into several pieces rather than turning into powder after compression test. For PEGDA-50%A200-4h, Al_2O_3-200 particles have a stable thermal stability and does not show an obvious change after calcination. For PEGDA-35%LTA-15%A200-4h, zeolite aggregates around Al_2O_3-200 particles, which results in a better contact between zeolite and Al_2O_3-200. This contact is probably more pronounced for 35:15 (LTA-5A : Al_2O_3-200) than 25:25 which could explain the higher structure strength of PEGDA-35%LTA-15%A200-4h to support a heavy wight on it top surface.

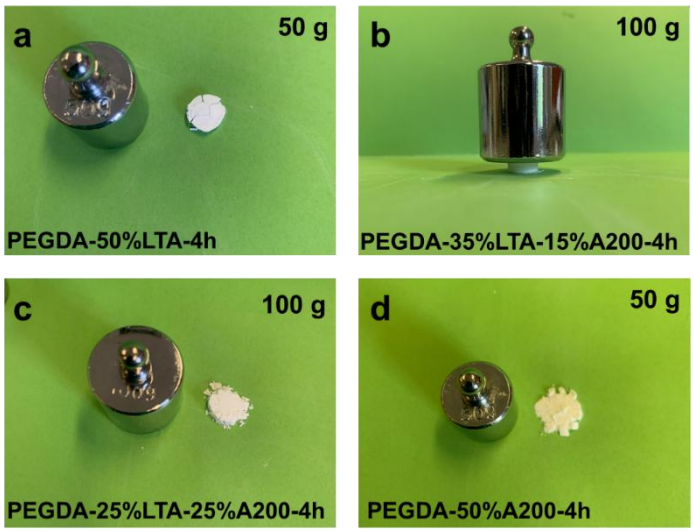

Fig. 9. Bear-loading tests on calcinated samples: (a) PEGDA-50%LTA-4h, (b) PEGDA-35%LTA-15%A200-4h, (c) PEGDA-25%LTA-25%A200-4h and (d) PEGDA-50%A200-4h.

4. Conclusion

In this work, three different types of monomers and five types of fillers were studied to obtain composites via photopolymerization (405 nm, mild conditions). All results demonstrated that

composite with LTA-5A had a higher value of depth of cure (DOC), and composites with Al_2O_3 had better mechanical properties. Hence, double filler-based composites (LTA-5A and Al_2O_3-200) were successfully prepared, which had good depth of cure (DOC) and good mechanical properties. After direct laser write (DLW), double filler-based composites had a good spatial resolution and have a good behavior in water swelling experiments. 4D printing behaviors were also manufactured through hydrothermal stimuli actuation of 3D printed composites. In addition, the 3D object with 4D printing condition could withstand a heavy stuff (more than 100 times its own mass) and without any damages. Calcined composites containing LTA-5A also kept the porosity and had a good CO_2 adsorption performance comparable to commercial LTA-5A beads. Therefore, this work not only paves the way for the investigation of photo-composites filled with multiple fillers combinations, but also shows us the potential applications in the field of 3D/4D printing, microlithography and functional composites. In addition, this work also gives a new approach to manufacture 3D zeolite monoliths (calcined composites) for gas adsorption application.

Credit authorship contribution statement

Yijun Zhang: Methodology, Validation, Formal analysis, Investigation, Data curation, Writing – original draft, Funding acquisition. **Yuanyuan GAO**: Validation, Formal analysis, Data curation. **Laure michelin**: Formal analysis (XRD), Data curation. **Ludovic Josien**: Formal analysis (SEM), Data curation. **Loïc Vidal**: Formal analysis (SEM), Data curation. **Gautier Schrodj**: Formal analysis (DMA, TGA), Data curation. **Angélique Simon-Masseron**: Conceptualization, Methodology, Validation, Formal analysis, Data curation, Writing - original draft, Supervision, Project administration. **Jacques Lalevée**: Conceptualization, Methodology, Validation, Formal analysis, Data curation, Writing - original draft, Supervision, Project administration, Funding acquisition.

Corresponding Authors

Angélique Simon-Masseron, angelique.simon-masseron@uha.fr

Jacques Lalevée, jacques.lalevee@uha.fr

Declaration of competing interest

The authors declare that they have no known competing financial interests or personal

relationships that could have appeared to influence the work reported in this paper.

Acknowledgments

The authors wish to acknowledge Dr. Séverinne Rigolet, engineer in Institut de Science des Matériaux de Mulhouse (IS2M), for her help in NMR experiments and analyses in this study.

Funding Sources

This work was supported by the Region Grand Est (France) for the grant “MIPPI-4D”.

Data Availability Statement

The raw/processed data required to reproduce these findings cannot be shared at this time due to technical or time limitations.

References

[1] Y. Zhang, Y. Xu, A. Simon-Masseron, J. Lalevee, Radical photoinitiation with LEDs and applications in the 3D printing of composites, Chem Soc Rev 50(6) (2021) 3824-3841.

[2] X. Wang, M. Jiang, Z. Zhou, J. Gou, D. Hui, 3D printing of polymer matrix composites: A review and prospective, Compos. Part B-Eng. 110 (2017) 442-458.

[3] S.J. Lee, W. Zhu, M. Nowicki, G. Lee, D.N. Heo, J. Kim, Y.Y. Zuo, L.G. Zhang, 3D printing nano conductive multi-walled carbon nanotube scaffolds for nerve regeneration, J. Neural. Eng. 15(1) (2018) 016018-016045.

[4] N.B. Palaganas, J.D. Mangadlao, A.C.C. de Leon, J.O. Palaganas, K.D. Pangilinan, Y.J. Lee, R.C. Advincula, 3D printing of photocurable cellulose nanocrystal composite for fabrication of complex architectures via stereolithography, ACS Appl. Mater. Inter 9(39) (2017) 34314-34324.

[5] C.W.J. Lim, K.Q. Le, Q. Lu, C.H. Wong, An overview of 3-D printing in manufacturing, aerospace, and automotive industries, IEEE Potentials 35(4) (2016) 18-22.

[6] A.J. Guerra, H. Lara-Padilla, M.L. Becker, C.A. Rodriguez, D. Dean, Photopolymerizable resins for 3D-printing solid-cured tissue engineered implants, Curr. Drug Targets 20(8) (2019) 823-838.

[7] J.-Y. Lee, J. An, C.K. Chua, Fundamentals and applications of 3D printing for novel materials, Appl. Mater. Today 7 (2017) 120-133.

[8] J.R. Tumbleston, D. Shirvanyants, N. Ermoshkin, R. Janusziewicz, A.R. Johnson, D. Kelly, K. Chen, R. Pinschmidt, J.P. Rolland, A. Ermoshkin, E.T. Samulski, J.M. DeSimone, Continuous liquid interface production of 3D objects, Science 347(6228) (2015) 1349-1352.

[9] A.I. Salimon, F.S. Senatov, V. Kalyaev, A.M. Korsunsky, Shape memory polymer blends and composites for 3D and 4D printing applications, 3D and 4D Printing of Polymer Nanocomposite Materials2020, pp. 161-189.

[10] A.S. Gladman, E.A. Matsumoto, R.G. Nuzzo, L. Mahadevan, J.A. Lewis,

Biomimetic 4D printing, Nat. Mater. 15(4) (2016) 413-418.

[11] Z. Zhang, N. Corrigan, A. Bagheri, J. Jin, C. Boyer, A versatile 3D and 4D printing system through photocontrolled raft polymerization, Angew. Chem. Int. Ed. Engl. 58(50) (2019) 17954 –17963.

[12] Z. Zhang, K.G. Demir, G.X. Gu, Developments in 4D-printing: a review on current smart materials, technologies, and applications, Int. J. Smart Nano. Mater. 10(3) (2019) 205-224.

[13] J. Choi, O.C. Kwon, W. Jo, H.J. Lee, M.-W. Moon, 4D printing technology: A review, 3D Print. Addit. Manuf. 2(4) (2015) 159-167.

[14] Y. Xia, Y. He, F. Zhang, Y. Liu, J. Leng, A review of shape memory polymers and composites: mechanisms, materials, and applications, Adv. Mater. 33(6) (2021) 2000713-2000745.

[15] M. Javaid, A. Haleem, 4D printing applications in medical field: A brief review, Clin. Epidemiology Glob. Health 7(3) (2019) 317-321.

[16] Y. Zhang, H. Chen, S. Liu, L. Josien, G. Schrodj, A. Simon-Masseron, J. Lalevée, Photopolymerization of pollen based biosourced composites and applications in 3D and 4D printing, Macromol. Mater. Eng. 306(6) (2021) 2000774-2000783.

[17] H. Chen, C. Regeard, H. Salmi, F. Morlet-Savary, N. Giacoletto, M. Nechab, P. Xiao, F. Dumur, J. Lalevée, Interpenetrating polymer network hydrogels using natural based dyes initiating systems: antibacterial activity and 3D/4D performance, Eur. Polym. J. 166 (2022) 111042-111057.

[18] S. Liu, D. Brunel, K. Sun, Y. Xu, F. Morlet-Savary, B. Graff, P. Xiao, F. Dumur, J. Lalevée, A monocomponent bifunctional benzophenone-carbazole type II photoinitiator for LED photoinitiating systems, Polym. Chem. 11(21) (2020) 3551-3556.

[19] H. Mokbel, B. Graff, F. Dumur, J. Lalevee, NIR sensitizer operating under long wavelength (1064 nm) for free radical photopolymerization processes, Macromol. Rapid Comm. 41(15) (2020) 2000289-2000293.

[20] C. Dietlin, S. Schweizer, P. Xiao, J. Zhang, F. Morlet-Savary, B. Graff, J.-P.

Fouassier, J. Lalevée, Photopolymerization upon LEDs: New photoinitiating systems and strategies, Polym. Chem. 6(21) (2015) 3895-3912.

[21] M.A. Tasdelen, J. Lalevée, Y. Yagci, Photoinduced free radical promoted cationic polymerization 40 years after its discovery, Polym. Chem. 11(6) (2020) 1111-1121.

[22] H. Chen, Y. Zhang, A. Bonfiglio, F. Morlet-Savary, M. Mauro, J. Lalevée, Rhenium(I) N-heterocyclic carbene complexes in photoinitiating systems for polymerization upon visible light: development of photosensitive resins for 3D and 4D applications, ACS Appl. Polym. Mater. 3(1) (2020) 464-473.

[23] S. Liu, Y. Zhang, K. Sun, B. Graff, P. Xiao, F. Dumur, J. Lalevée, Design of photoinitiating systems based on the chalcone-anthracene scaffold for LED cationic photopolymerization and application in 3D printing, Eur. Polym. J. 147 (2021) 110300-110308.

[24] S. Liu, H. Chen, Y. Zhang, K. Sun, Y. Xu, F. Morlet-Savary, B. Graff, G. Noirbent, C. Pigot, D. Brunel, M. Nechab, D. Gigmes, P. Xiao, F. Dumur, J. Lalevee, Monocomponent photoinitiators based on benzophenone-carbazole structure for LED photoinitiating systems and application on 3D printing, Polymers 12(6) (2020) 1394-1408.

[25] P. Garra, J.P. Fouassier, S. Lakhdar, Y. Yagci, J. Lalevée, Visible light photoinitiating systems by charge transfer complexes: photochemistry without dyes, Prog. Polym. Sci. 107 (2020).

[26] Y. Zhang, Y. Gao, L. Josien, H. Nouali, C. Vaulot, A. Simon- Masseron, J. Lalevée, Photopolymerization of zeolite filler- based composites for potential 3D printing application and gas adsorption applications, Adv. Mater. Technol. 7(3) (2022) 2100869-2100879.

[27] T.E. Glier, L. Akinsinde, M. Paufler, F. Otto, M. Hashemi, L. Grote, L. Daams, G. Neuber, B. Grimm-Lebsanft, F. Biebl, D. Rukser, M. Lippmann, W. Ohm, M. Schwartzkopf, C.J. Brett, T. Matsuyama, S.V. Roth, M. Rubhausen, Functional printing of conductive silver-nanowire photopolymer composites, Sci. Rep. 9(1) (2019) 1-7.

[28] S.P. Gentry, J.W. Halloran, Light scattering in absorbing ceramic suspensions: Effect on the width and depth of photopolymerized features, J. Eur.Ceram. Soc. 35(6) (2015) 1895-1904.

[29] C. Baerlocher, L.B. McCusker, D.H. Olson, Atlas of zeolite framework types, Elsevier2007.

[30] H. Zhang, P. Wang, H. Zhang, H. Yang, H. Wang, L. Zhang, Structured zeolite monoliths with ultrathin framework for fast CO_2 adsorption enabled by 3D printing, Ind. Eng. Chem, Res. 59(17) (2020) 8223-8229.

[31] H. Thakkar, S. Eastman, A. Hajari, A.A. Rownaghi, J.C. Knox, F. Rezaei, 3D-printed zeolite monoliths for CO_2 removal from enclosed environments, ACS Appl. Mater. Inter 8(41) (2016) 27753-27761.

[32] X. Li, W. Li, F. Rezaei, A. Rownaghi, Catalytic cracking of n-hexane for producing light olefins on 3D-printed monoliths of MFI and FAU zeolites, Chem. Eng. J. 333 (2018) 545-553.

[33] C.P. Spatarelu, A.L. Radu Chiriac, B. Cursaru, T.V. Iordache, A.M. Gavrila, C.T. Cojocaru, R.E. Botez, B. Trica, A. Sarbu, M. Teodorescu, V. Tofan, F.X. Perrin, A. Zaharia, Composite nanogels based on zeolite-poly(ethylene glycol) diacrylate for controlled drug delivery, Nanomaterials 10(2) (2020) 195-214.

[34] Y. Zhang, L. Josien, J.-P. Salomon, A. Simon-Masseron, J. Lalevée, Photopolymerization of zeolite/polymer-based composites: Toward 3D and 4D printing applications, ACS Appl. Polym. Mater. 3(1) (2020) 400-409.

[35] J. Lefevere, B. Claessens, S. Mullens, G. Baron, J. Cousin-Saint-Remi, J.F.M. Denayer, 3D-printed zeolitic imidazolate framework structures for adsorptive separations, ACS Appl. Nano Mater. 2(8) (2019) 4991-4999.

[36] Y. Zhang, S. Liu, H. Chen, L. Josien, G. Schrodj, A. Simon-Masseron, J. Lalevée, Development of a zeolite/polymer-based hydrogel composite through photopolymerization for 3D printing application, Macromol. Mater. Eng. 306(8) (2021) 2100129-2100135.

[37] O. Halevi, T.-Y. Chen, P.S. Lee, S. Magdassi, J.A. Hriljac, Nuclear wastewater

decontamination by 3D-printed hierarchical zeolite monoliths, RSC Adv. 10(10) (2020) 5766-5776.

[38] Z. Okulus, M. Sandomierski, M. Zielinska, T. Buchwald, A. Voelkel, Zeolite fillers for resin-based composites with remineralizing potential, Spectrochim. Acta A Mol. Biomol. Spectrosc. 210 (2019) 126-135.

[39] H. Xing, B. Zou, Q. Lai, C. Huang, Q. Chen, X. Fu, Z. Shi, Preparation and characterization of UV curable Al_2O_3 suspensions applying for stereolithography 3D printing ceramic microcomponent, Powder Technol. 338 (2018) 153-161.

[40] J.S. Yun, T.-W. Park, Y.H. Jeong, J.H. Cho, Development of ceramic-reinforced photopolymers for SLA 3D printing technology, Applied Physics A 122(6) (2016) 1-6.

[41] S.Y. Song, M.S. Park, D. Lee, J.W. Lee, J.S. Yun, Optimization and characterization of high-viscosity ZrO_2 ceramic nanocomposite resins for supportless stereolithography, Mater. Des. 180 (2019) 107960-107968.

[42] V. Promakhov, A. Zhukov, Y. Dubkova, I. Zhukov, S. Kovalchuk, T. Zhukova, A. Olisov, V. Klimenko, N. Savkina, Structure and properties of ZrO_2-20%Al_2O_3 ceramic composites obtained using additive technologies, Materials (Basel) 11(12) (2018) 2361-2372.

[43] Y. Hazan, K. Faber, Porous ceramics, ceramic/polymer, and metal-doped ceramic/polymer nanocomposites via freeze casting of photo-curable colloidal fluids, J. Am. Ceram. Soc. 95(1) (2012) 177-187.

[44] Z. Chen, Z. Li, J. Li, C. Liu, C. Lao, Y. Fu, C. Liu, Y. Li, P. Wang, Y. He, 3D printing of ceramics: A review, J. Eur.Ceram. Soc. 39(4) (2019) 661-687.

[45] E. Castro e Costa, J.P. Duarte, P. Bártolo, A review of additive manufacturing for ceramic production, Rapid Prototyping J. 23(5) (2017) 954-963.

[46] A. Wieclaw- Midor, P. Falkowski, M. Szafran, Influence of core- shell structure on the cure depth in photopolymerizable alumina dispersion, Int. J. Appl. Ceram. Technol. 17(1) (2019) 248-254.

[47] B. Howard, N.D. Wilson, S.M. Newman, C.S. Pfeifer, J.W. Stansbury, Relationships between conversion, temperature and optical properties during

composite photopolymerization, Acta Biomater. 6(6) (2010) 2053-2059.

[48] G.B. Dos Santos, R.V. Alto, H.R. Filho, E.M. Da Silva, C.E. Fellows, Light transmission on dental resin composites, Dent. Mater. 24(5) (2008) 571-576.

[49] S. Westbeek, J.A.W. van Dommelen, J.J.C. Remmers, M.G.D. Geers, Influence of particle shape in the additive manufacturing process for ceramics, Comput. Math. Appl. 78(7) (2019) 2360-2376.

[50] K. Fujita, T. Ikemi, N. Nishiyama, Effects of particle size of silica filler on polymerization conversion in a light-curing resin composite, Dent. Mater. 27(11) (2011) 1079-1085.

[51] F. Kundie, C.H. Azhari, A. Muchtar, Z.A. Ahmad, Effects of Filler Size on the Mechanical Properties of Polymer-filled Dental Composites: A Review of Recent Developments, Journal of Physical Science 29(1) (2018) 141-165.

[52] H.M. Hassanabadi, D. Rodrigue, Effect of Particle Size and Shape on the Reinforcing Efficiency of Nanoparticles in Polymer Nanocomposites, Macromol. Mater. Eng. 299(10) (2014) 1220-1231.

[53] S.-Y. Fu, X.-Q. Feng, B. Lauke, Y.-W. Mai, Effects of particle size, particle/matrix interface adhesion and particle loading on mechanical properties of particulate–polymer composites, Compos. Part B-Eng. 39(6) (2008) 933-961.

[54] K. Jung, N. Corrigan, M. Ciftci, J. Xu, S.E. Seo, C.J. Hawker, C. Boyer, Designing with light: advanced 2D, 3D, and 4D materials, Adv. Mater. 32(18) (2020) 1903850-1903870.

[55] M. Piedrahita-Bello, J.E. Angulo-Cervera, R. Courson, G. Molnár, L. Malaquin, C. Thibault, B. Tondu, L. Salmon, A. Bousseksou, 4D printing with spin-crossover polymer composites, J. Mater. Chem. C 8(18) (2020) 6001-6005.

[56] Z. Xue, J. Ma, W. Hao, X. Bai, Y. Kang, J. Liu, R. Li, Synthesis and characterization of ordered mesoporous zeolite LTA with high ion exchange ability, J. Mater. Chem. 22(6) (2012) 2532-2538.

[57] A.G. Stepanov, Basics of Solid-State NMR for Application in Zeolite Science, Zeolites and Zeolite-Like Materials2016, pp. 137-188.

[58] M. Haouas, F. Taulelle, C. Martineau, Recent advances in application of (27)Al NMR spectroscopy to materials science, Prog. Nucl. Magn. Reson. Spectrosc. 94-95 (2016) 11-36.

[59] I.V. Baklanova, V.N. Krasil'nikov, A.P. Tyutyunnik, Y.V. Baklanova, Precursor technology for the production of white and color phosphors based on Al_2O_3:Ln (Ln=Eu^{3+}, Tb^{3+} or Eu^{3+}/Tb^{3+}), J. Solid State Chem. 292 (2020) 121699-121709.